



Strain incompatibility and residual strains in ferroelectric single crystals

SUBJECT AREAS:

ACTUATORS

MATERIALS FOR DEVICES

FERROELECTRICS AND
MULTIFERROICS

ELECTRONIC PROPERTIES AND
MATERIALS

A. Pramanick¹, J. L. Jones², G. Tutuncu², D. Ghosh², A. D. Stoica¹ & K. An¹

¹Chemical and Engineering Materials Division, Oak Ridge National Laboratory, Oak Ridge, TN, ²Department of Materials Science and Engineering, University of Florida, Gainesville, FL.

Residual strains in ferroelectrics are known to adversely affect the material properties by aggravating crack growth and fatigue degradation. The primary cause for residual strains is strain incompatibility between different microstructural entities. For example, it was shown in polycrystalline ferroelectrics that residual strains are caused due to incompatibility between the electric-field-induced strains in grains with different crystallographic orientations. However, similar characterization of cause-effect in multidomain ferroelectric single crystals is lacking. In this article, we report on the development of plastic residual strains in [111]-oriented domain engineered BaTiO₃ single crystals. These internal strains are created due to strain incompatibility across 90° domain walls between the differently oriented domains. The average residual strains over a large crystal volume measured by *in situ* neutron diffraction is comparable to previous X-ray measurements of localized strains near domain boundaries, but are an order of magnitude lower than electric-field-induced residual strains in polycrystalline ferroelectrics.

Received
24 September 2012

Accepted
2 November 2012

Published
5 December 2012

Correspondence and requests for materials should be addressed to A.P. (pramanicka@ornl.gov) or K.A. (kean@ornl.gov)

Ferroelectric oxides are used in many electromechanical devices for sensors, actuators, medical imaging and energy-harvesting applications, owing to the large values of their piezoelectric coefficients¹. However several reliability issues could be the limiting factors against their applications in many cases. For example, polarization fatigue and cracking under electromechanical loading have limited applications of ferroelectric single crystals in the past^{2,3}. Recently, interest in single crystal ferroelectrics has been renewed due to the dramatic enhancement of their electromechanical properties with domain-engineering^{4,5}. It is therefore imperative that the factors that could undermine reliability of domain-engineered ferroelectric crystals be well characterized. It is known that in brittle ceramics such as BaTiO₃, internal crack growth is driven by residual strains generated between the different microstructural constituents under the application of electric fields⁶. These internal cracks could further aggravate fatigue degradation during repeated electrical cycling⁷. Characterization of residual strains in domain-engineered single crystals is therefore desirable. Although generation of residual strains in polycrystalline ferroelectric ceramics upon electromechanical loading is well characterized, corresponding studies in single crystals has been absent. This is more concerning as large internal strain mismatch is expected between the domains of different crystallographic orientations in domain-engineered crystals due to their anisotropic piezoelectric properties⁸. In this study, using *in situ* neutron diffraction we have characterized the plastic residual strains and inhomogeneous strain fields in [111]-oriented, domain-engineered BaTiO₃ single crystals caused due to interdomain strain incompatibilities during electric field application.

Domain-engineered ferroelectric crystals are created by the application of a sufficiently large electric field along a certain crystallographic axis other than the equilibrium zero-field polar axis. This process creates a set of domains whose polarization directions have a common angle with respect to the poling direction⁹. This is illustrated in Figure 1(a) for a tetragonal multidomain crystal, where the [111] direction is parallel to the electric field and the orthogonal <001> directions of the different possible domain orientations are equally misoriented with respect to the applied electric field. Please note that the direction [111] is different than the equilibrium zero-field polar axis of [001] in tetragonal BaTiO₃. In this sense, the term ‘poling’ here does not equate to its conventional meaning whereby the ferroelectric domains are reoriented so that their [001] axis is parallel to the applied electric field; rather it simply refers to the application of a large electric field to a crystal in the as-synthesized condition. The exact microstructural changes during this ‘poling’ process in domain-engineered crystals remain unclear, although formation of engineered domain configuration in tetragonal BaTiO₃ has been demonstrated for applied electric fields along [111]¹⁰. Nevertheless, the enhancement in piezoelectric properties of domain-engineered crystals has been variously attributed to polarization rotation¹¹ and/or susceptibility to shear deformation¹².

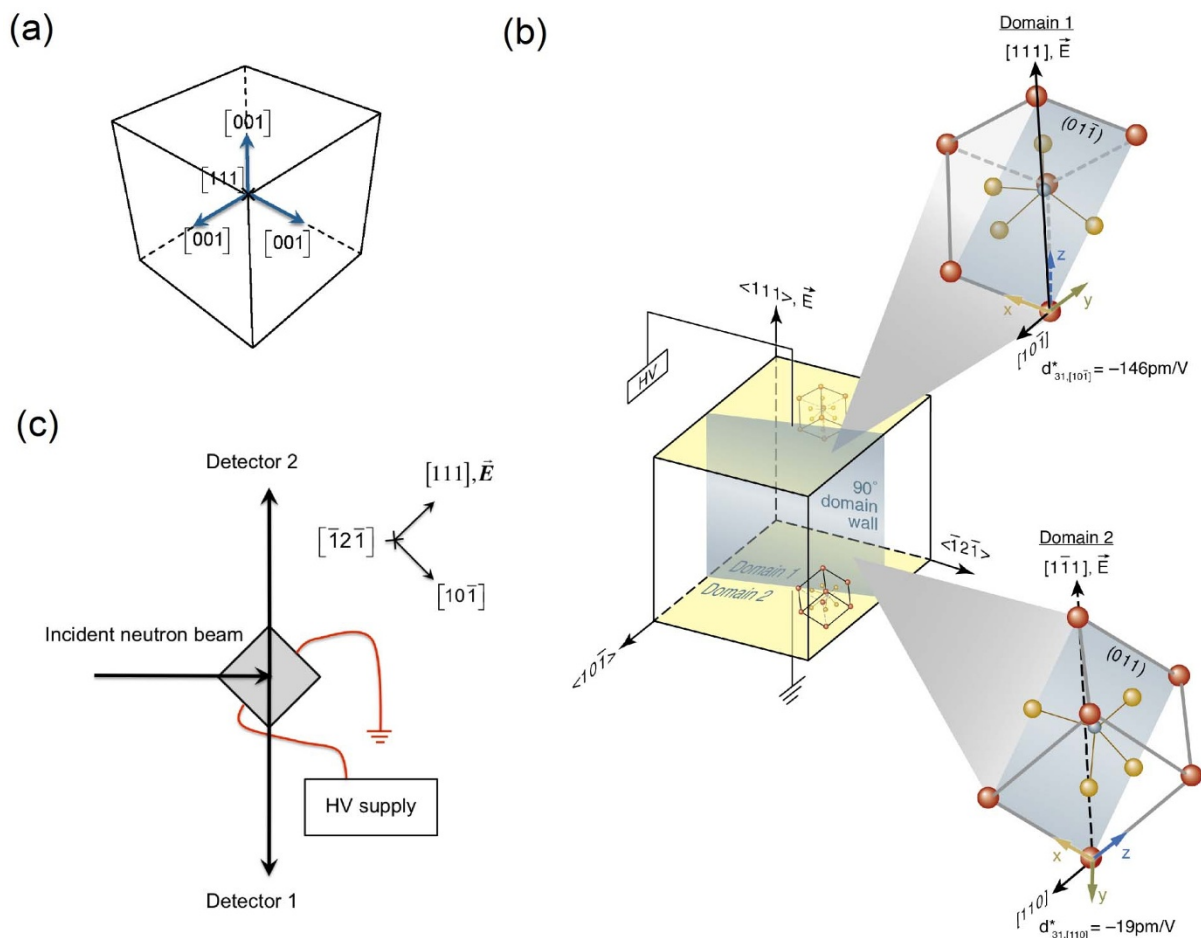


Figure 1 | Crystallographic orientations of domains and experimental set-up: (a) Schematic of domain engineered configuration of [111]-oriented single crystal. The pseudocubic [111] direction is equally oriented with respect to the [001] axes of the three orthogonal domain variants. (b) A split-view of two adjacent domains across a representative 90° domain wall within [111]-oriented domain-engineered BaTiO₃ single crystal. Many such domain walls can exist within a crystal, a representation of which is shown here. Electric field is applied parallel to 111 plane normals; while transverse electric-field-induced structural changes are indicated parallel to [101] and [110] for Domain 1 and Domain 2, respectively. The misfit in the transverse electric-field-induced strain responses of the two domains, as indicated by their d_{31}^* responses, creates an incompatibility in the domain wall region. In the schematic, Domain 1 is behind the 90° domain wall and Domain 2 is in front of the 90° domain wall. The spontaneous polarization is parallel to the \bar{z} direction in the two domains. (c) Schematic of *in situ* neutron diffraction experiment on domain-engineered BaTiO₃ crystal, electric field is applied parallel to [111]. All crystallographic coordinates in the schematic are given in pseudocubic notation. (schematic courtesy René Manning).

A particular concern in domain-engineered crystals is the effect of strain incompatibilities between the adjacent domains across non-180° domain boundaries under electromechanical loading. The present work presents a prototypical analysis of this loading scenario, wherein a large difference in the electric-field-induced strains exists between the two degenerate pseudocubic directions in strongly anisotropic BaTiO₃, as shown in Figure 1(b). In this configuration, for both domains, the electric field is applied parallel to the direction normal to the (111)-type planes. For Domain 1, the direction transverse to the applied electric field is [101]. Correspondingly, for Domain 2, the direction transverse to the applied electric field is [110]. In this geometry, the transverse d_{31}^* coefficient corresponding to strain parallel to [101] for Domain 1 is -146 pm/V , and the transverse d_{31}^* coefficient corresponding to strain parallel to [110] for Domain 2 is -19 pm/V . The notation d_{31}^* denotes the transverse coefficient along a certain crystallographic direction such as [110] and should be distinguished from the macroscopic transverse piezoelectric coefficient of a crystal, d_{31} . In domain-engineered BaTiO₃, the large mismatch in the transverse piezoelectric coefficients d_{31}^* of the adjacent domains along [110]-type directions is expected to create an electric-field-induced strain mismatch in the domain wall

region. For an applied electric field of 500 V/mm, the difference in d_{31}^* coefficients creates a strain mismatch of $\sim 0.006\%$ between the domains, which is of the same order of the total electric-field-induced strain of the crystal itself. The mismatch between the induced strains in domains of two different orientations must be accommodated within the microstructure.

The resolution of strain (in)compatibilities between the different components of an aggregate microstructure containing crystallites with different orientations is a classic problem in materials science. When the adjacent crystallites across a coherent interface exhibit strain mismatch as a result of elastic or plastic anisotropies, internal stresses are induced to maintain compatibility. Such internally generated stresses, which act in addition to external forces, are called compatibility stresses¹³. Examples of compatibility stresses can be found at interfaces between metallic bicrystals^{13,14}, at twin boundaries in ferroelastic oxides¹⁵, and at interfaces between epitaxial thin films and substrates¹⁶. When a sufficiently large strain gradient is induced across a coherent interface, compensating dislocations are formed which locally relieve the compatibility stresses. The compensating dislocations, while creating local discontinuities, enhance the overall coherency of the interface and minimize the strain energy at the



interface due to elastic mismatch^{13–16}. In ferroelectric materials, domain walls are the examples of coherent interfaces wherein compatibility stresses can arise due to difference in piezoelectric responses of the adjacent domains¹. The result of such compatibility stresses in domain-engineered crystals is of interest here.

In the last decade, nanoscale details about the domain structures in ferroelectric materials have come forth due to the improved resolution of different microscopy techniques. Recent examples include use of Piezoresponse Force Microscope (PFM) to reveal the mesoscopic dipole closure patterns in single-crystal BaTiO₃¹⁷, and use of aberration-corrected transmission electron microscope (TEM) to study localized nucleation and growth of ferroelectric domains in BiFeO₃ thin films¹⁸. A rather extensive review of recent findings on nanoscale domain patterns in ferroelectrics can be found in Catalan et al¹⁹. Although powerful, these microscopy techniques lack quantitative information regarding the residual crystallographic strains in ferroelectric domain structures, and only indirect information about local strain states can be obtained from polarization loops measured with PFM²⁰. In comparison, scanning diffraction experiments with high-energy microfocused or nanofocused X-rays have provided much greater insights regarding the strain fields around domain walls in ferroelectric single crystals^{21–23}. However, scanning based techniques with either pointed tips or X-rays are not suitable for dynamic measurements during *in situ* electric field application because the position of interest changes with domain wall motion²⁴. Moreover, scanning diffraction experiments can only provide strain information at a particular local point and elucidating residual strains over larger sample volumes would require a statistical analysis of several different measurements. Therefore, it would be much more advantageous if internal strains in ferroelectric domain structures could be revealed from diffraction measurements taken with a large beam that is comparable in size with the material of interest.

In this study our objective is to investigate the evolution of *internal strain fields* in [111]-oriented and domain-engineered BaTiO₃ ferroelectric crystals during and subsequent to the application of electric fields. The strain fields arise due to alterations in the atomic-scale structure that are readily measured in diffraction. *In situ* neutron diffraction of single crystals under applied electric fields provides volume-averaged information of strain states across multiple domains and the evolution of internal strain fields can be ascertained from such information, as shown here. The particular advantage of neutron diffraction is that neutrons penetrate deep inside a sample and therefore probes structural changes inside the bulk of a material. BaTiO₃ is chosen in the present work to serve as a prototypical ferroelectric in which to observe the effects of strain mismatch and, moreover, to avoid the structural complexities that could arise in relaxor ferroelectrics due to a coexistence of polar nanoregions and multiple ferroelectric phases^{25–27}.

Results

The experimental setup for *in situ* diffraction under applied electric fields is illustrated in Figure 1(c). The BaTiO₃ crystals were obtained in their as-processed state and subjected to the electric fields for the first time during the current experiment. Two different crystals were used, one of which was subjected to positive electric fields and another to negative electric fields. The neutrons diffracted from the sample were measured on 2-D area detectors (see Supplementary Information for details). All *in situ* neutron diffraction measurements were taken for applied field amplitudes of greater than (+/−) 100 V/mm, which is the nominal coercive field for tetragonal BaTiO₃ single crystals^{10,28}.

Structural changes measured parallel to applied electric field.

Representative changes in the integrated 333 diffraction peak profile upon application of positive and negative electric fields are shown in Figures 2(a) and 2(b), respectively. The 333 momentum

transfer vector for neutron diffraction is parallel to the direction of the applied electric field, and therefore provides measurement of crystallographic changes parallel to the applied field direction. In both cases, with increase in field amplitude, the 333 peak position shifts towards higher *d*-spacing, along with an increase in total peak intensity. Electric-field-induced changes in the (333) interplanar *d*-spacing, Δd , are calculated with respect to the *d*-spacing measured at a certain minimum field amplitude of (+/−) 100 V/mm. As shown in Figure 2(c), Δd increases linearly with increase in electric field amplitude for both samples, except for the field amplitude of 275 V/mm, at which point a sharp discontinuity in Δd is evident for the sample subjected to positive electric fields. No such discontinuity is observed for the crystal subjected to negative electric fields. Linear fits to Δd yield corresponding electric-field-induced strain coefficients of 678 pm/V and 845 pm/V, for the crystals subjected to positive and negative electric fields, respectively. These values of strain coefficients are more than 3 times the values of d_{33}^* parallel to the 111 crystallographic direction (~ 200 pm/V), as calculated from the coefficients of single crystalline piezoelectric tensor of BaTiO₃¹² or reported from macroscopic measurements²⁹. This indicates that the measured electric-field-induced 333 lattice strains observed here are more complex than the intrinsic piezoelectric strain of the lattice suggests.

The normalized 333 peak intensities are plotted as A_{111}^E/A_{111}^0 in Figure 2(d), where A_{111}^E refers to the integrated 333 peak intensity for an applied electric field amplitude *E* and A_{111}^0 refers to the integrated 333 peak intensity for an applied electric field amplitude of (+/−) 100 V/mm. Figure 2(d) shows that the 333 peak intensity increases linearly with an increase in the amplitude of negatively polarized electric field. However, the crystal subjected to positive electric field shows a minimal change by comparison. Notably, a sharp discontinuity in the 333 integrated peak intensity can be observed at the field amplitude of 275 V/mm, which correlates with the trend observed for Δd for the crystal subjected to positive electric fields.

Structural changes measured transverse to applied electric field.

Representative changes in 220 diffraction peak profiles upon application of electric fields are shown in Figures 3(a) and 3(b). The 220 momentum transfer vector lies orthogonal to the direction of the applied electric field, and therefore provides measurement of crystallographic changes transverse to the applied field direction. The results for the normalized peak intensities are represented as A_{220}^E/A_{220}^0 in Figure 3(c), where the superscripts have the same meaning as for the normalized 333 diffraction peak intensities. The change in integrated 220 peak intensities is larger for the crystal subjected to negative electric fields as compared to the crystal subjected to positive electric fields. Also, consistent with the trend observed in Figure 2(d), Figure 3(c) shows a sharp discontinuity in the integrated 220 peak intensity at 275 V/mm for the sample subjected to positive electric field. It is important to note that the observed intensity changes for the 220 diffraction peaks are different from intensity interchange observed normally between degenerate diffraction peaks in ferroelectric materials that are characteristic of change in volume fraction of non-180° domains³⁰. In fact, the peak corresponding to the reflecting planes normal to the [220] direction exhibits greater change in intensity as compared to the peak corresponding to the reflecting planes normal to the [20 $\bar{2}$] direction. Therefore, it is unlikely that the intensity change for the 220 diffraction peaks observed here is due to non-180° domain switching. The origins of the measured lattice strains and peak intensity changes are examined in the following discussion.

Discussion

As shown in the schematic in Figure 1(b), the direction normal to the (*hhh*) planes is parallel to the (*kk0*)-type planes that correspond to the 90° domain walls²⁹. Therefore, during the application of electric

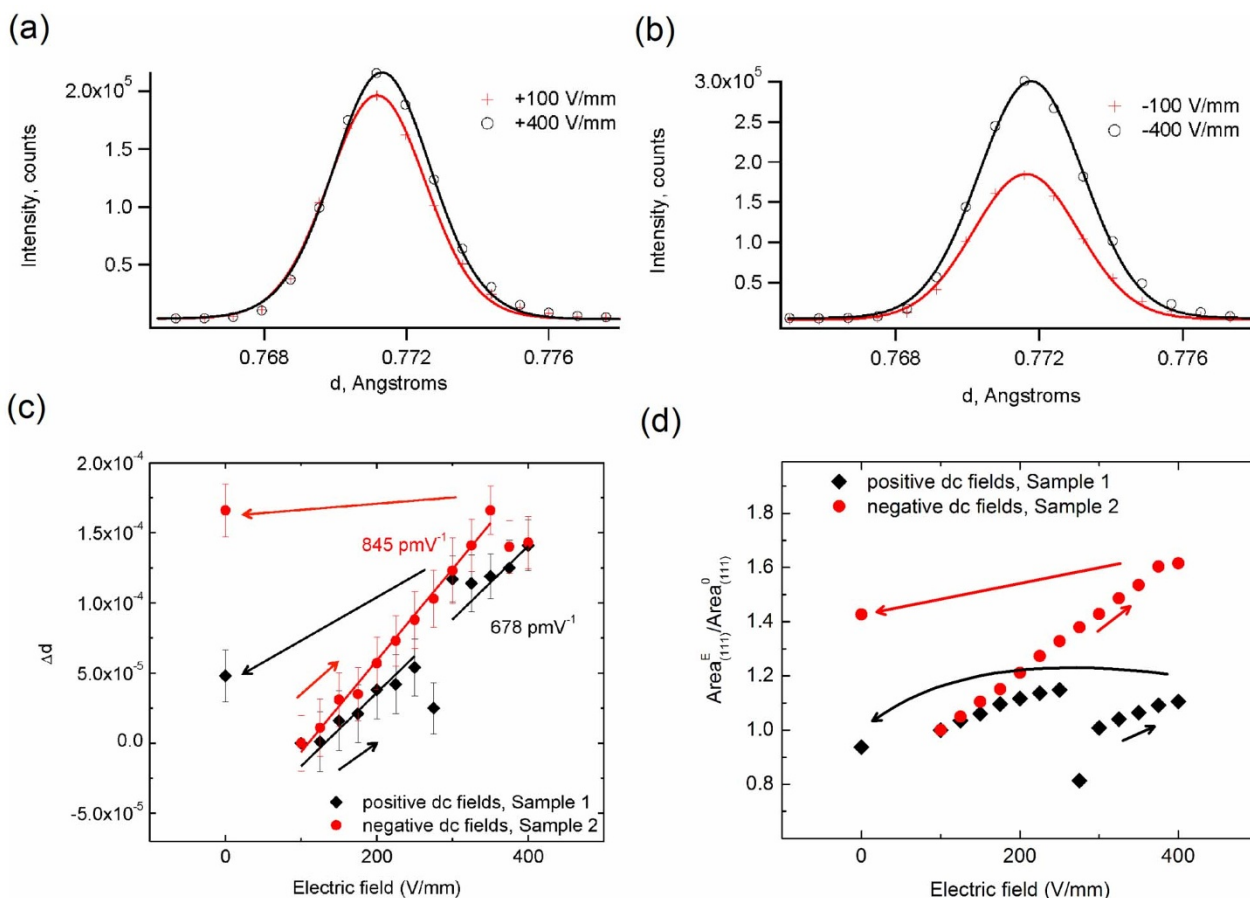


Figure 2 | Electric-field-induced structural changes parallel to direction of applied electric field: (a),(b) changes in 333 diffraction peak profiles for the crystal subjected to (a) positive, and (b) negative electric fields; (c) change in (333) lattice plane spacing, Δd , as function of applied electric field amplitude; (d) change in integrated intensity of 333 diffraction peaks as function of electric field amplitude. The arrows indicate the directions of progressive changes in the applied electric field. The final datapoint is measured at zero field subsequent to the application of a large electric field.

fields, the internal compatibility stresses arising from a strain mismatch across 90° domain walls causes straining of the (*hhh*)-type planes, which is evident from Figure 3(c). The corresponding lattice strains are calculated from the data shown in Figure 3. A maximum (*hhh*) lattice strain ($\Delta d/d$) of $\sim 2 \times 10^{-4}$ is observed for an applied field amplitude of 400 V/mm. Additionally, subsequent to the electric field application, a residual strain of $\sim 7 \times 10^{-5}$ is observed for the crystal subjected to positive electric fields, and a corresponding residual strain of $\sim 2 \times 10^{-4}$ is observed for the crystal subjected to negative electric fields. These values of residual (*hhh*) lattice strains are comparable to the zero-field (002) lattice strains of $\sim 7 \times 10^{-5}$ measured with microfocused X-rays around 90° domain walls in tetragonal BaTiO₃ crystals²¹. In comparison, residual (*hhh*) lattice strains of $\sim 10^{-3}$ were reported for polycrystalline lead zirconate titanate (PZT) ceramics subsequent to electric field application³¹. A higher residual strain in polycrystalline PZT could be due to the higher piezoelectric coefficients of soft PZT materials as compared to that of tetragonal BaTiO₃. On the other hand, while the piezoelectric coefficients of PZT are higher by about a factor of five, the residual lattice strains measured in polycrystalline PZT is more than an order of magnitude higher than the corresponding lattice strain values measured here for BaTiO₃ single crystals. This likely suggests that the presence of grain boundaries enhances the residual strains in ferroelectric materials.

It was observed earlier in polycrystalline tetragonal ferroelectrics that strain mismatch between the neighboring grains causes residual elastic strains for the (*hhh*)-type lattice planes³¹. The residual *hhh* elastic lattice strain for a set of similarly oriented grains (measured

subsequent to electric field application) can be either positive or negative, depending on their specific crystallographic orientations. However, the net elastic strain integrated over all the grains vanishes due to the stress balance condition and the assumed uniform elastic constant³². This situation can be compared with the present case wherein a strain mismatch exists between the differently oriented domains in a single crystal sample. For single crystal diffraction, the *hhh* poles from all the domains are measured along a single direction. Therefore, the overall measured 333 lattice strain is a volume-average of the 333 lattice strains of all the domains, which includes domains on both sides of the 90° domain walls. In this situation, based on internal stress balance condition, no residual elastic lattice strains should be observed at zero electric field if the internal strain fields across 90° domain walls are symmetric. The fact that a residual *hhh* elastic lattice strain is measured subsequent to electric field application indicates a generation of asymmetric internal strain fields across 90° domain walls. Moreover, it also shows a certain degree of plastic deformation within the crystal.

In addition to changes in lattice *d*-spacing, internal gradients of lattice distortions in single crystal samples also result in an increase of diffraction peak intensities, as was previously observed in ferroelectric crystals upon application of electric fields^{27,33}. The currently observed changes in diffraction peak intensities can be similarly attributed to the evolution of internal strain gradients. The differently oriented domains with orthogonal polarization vectors across 90° domain walls give rise to the two degenerate Bragg peaks for the 220 reflection. It is observed here that as an effect of electric field application, these two peaks exhibit disproportionate changes in

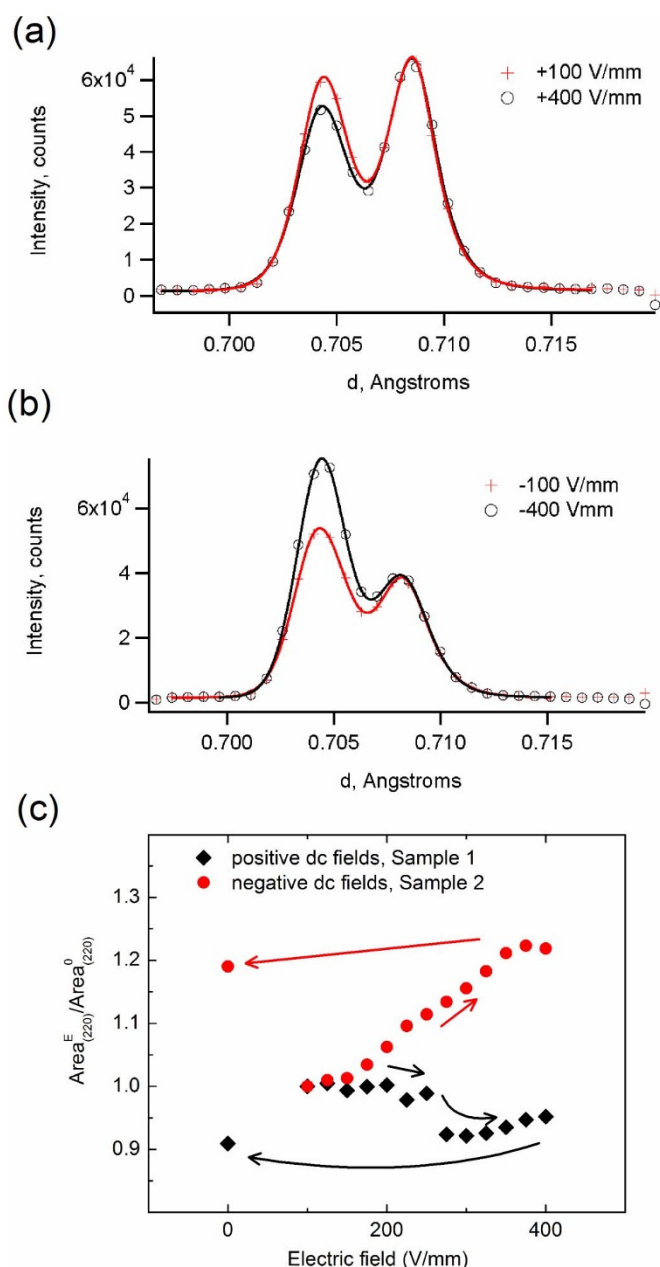


Figure 3 | Electric-field-induced structural changes transverse to the direction of applied electric field: changes in 220 diffraction peak profile for crystals subjected to (a) positive, and (b) negative electric fields; (c) change in integrated intensity of 220 diffraction peaks as function of electric field amplitude. The arrows indicate the directions of progressive changes in the applied electric field. The final datapoint is measured at zero field subsequent to the application of a large electric field.

peak intensities (Figure 3(a) and (b)). This indicates that the internal strain gradients on either side of the 90° domain walls are not symmetric. This view is consistent with the earlier assertion that asymmetric strain fields across 90° domain walls are also the cause for the observed residual 333 lattice strains. In fact, we observe an exact correlation between the residual 333 lattice strains and the increase in diffraction peak intensities - the sample that shows a larger residual strain also exhibits a larger increase in 220 and 333 peak intensities. A hypothetical case where a 90° domain wall can have an asymmetric strain profile is schematically illustrated in Figure 4.

Previous microdiffraction experiments on single crystals indeed showed that some components of deviatoric strain tensors exhibit

asymmetry as a function of position around a 90° domain wall, even under zero electric fields²². Such strain asymmetries were also reported along twin boundaries in germanium bicrystals due to the presence of dislocations³⁴. Strain asymmetries can arise due to a difference in the stiffness of the compressed and expanded regions around a dislocation along the twin boundaries, which in turn depends on the local atomic arrangements at the interface³⁴. It can be debated whether dislocations are also responsible for asymmetric strain fields across 90° domain walls, although that scenario seems likely in the present case. Since the transverse strains of the adjacent domains differ by a factor of ~ 7 , there is a large strain mismatch in the 90° domain wall area and this consequently increases the local strain energy. The strain energy near 90° domain walls can be potentially reduced due to interaction between the strain fields of dislocations with Burger's vector $\vec{b} // \langle 110 \rangle$ and those of 90° domain walls, as recently shown by phase-field modeling³⁵. It is therefore possible that the increased strain energy due to interdomain strain incompatibility is partially relieved by new dislocations created along 90° domain walls. This is one possible explanation for the electric-field-induced residual strains in domain-engineered BaTiO₃ crystals. Additionally, the inhomogeneous field distribution near the 90° domain wall due to non-uniform dielectric response could also be a contributing factor for strain asymmetries near 90° domain walls. For further insights, it will be interesting to look at the microscopic length scales over which the internal strains are distributed around the domain wall region in domain-engineered crystals. It is expected that future experiments with micro/nano focused X-rays can provide such information.

The reason for the slightly different strain behavior of the two samples is not entirely clear, although multiple effects could be contributing to this such as extension (sample subjected to negative electric field) vs. compression (sample subjected to positive electric field) of the crystal in the transverse direction, or presence of pre-existing defects along the domain walls. Nevertheless, the subtle differences in the structural changes observed for the two different samples suggest that the electric-field-induced structural changes in ferroelectric single crystals are highly sensitive to the existent local imperfections and their evolution under applied electric fields.

The connection between interdomain residual strains and performance of ferroelectric single crystals is an area that needs further

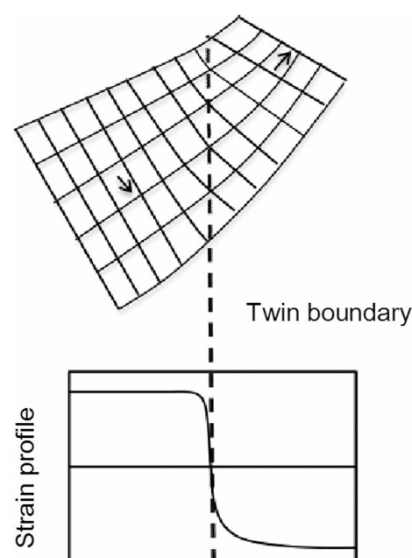


Figure 4 | Domain-wall with asymmetric strain profile: The proposed structure of a 90° domain wall with an asymmetric strain profile across it. The arrows indicate the direction of polarization vector for the two domains.



clarification. Future research efforts should be directed to understand effects of residual strains on time-dependent and fatigue behavior of multidomain single-crystalline functional materials.

Methods

Two single crystals of BaTiO₃ in the engineered domain configuration were obtained from Mateck GmbH. The two crystals were obtained from two different processing batches. The crystals were cut so that their face normals were parallel to the orthogonal (111), (101) and $\langle 1\bar{2}1 \rangle$ directions, and electric field was applied across the crystal faces normal to the (111) direction. *In situ* structural measurements during the application of electric fields were obtained at the newly commissioned VULCAN Engineering Diffractometer of the Spallation Neutron Source at the Oak Ridge National Laboratory³⁶. The structural changes in the two different crystals under opposite polarities of applied electric fields were measured. In one sample, the amplitude of the positively polarized electric field was increased stepwise with increments of 25 V/mm, starting from (+) 100 V/mm up to a maximum field of (+) 400 V/mm. In the second sample, the amplitude of the negatively polarized electric field was increased from (−) 100 V/mm up to a maximum field of (−) 400 V/mm, in steps of 25 V/mm. Neutrons diffracted from the crystal are measured by the two area detectors placed at 180° degrees with respect to each other. The vertical axes of the two detectors in the laboratory 3-D space are parallel to the $\langle 11\bar{2} \rangle$ crystallographic directions, while the horizontal axes of the detectors are in the plane containing the (111) and (101) the crystallographic directions. Therefore, the two area detectors of the diffractometer measure diffraction peaks in the time-of-flight mode, with their momentum transfer vectors approximately parallel to the orthogonal (111) and $\langle 10\bar{1} \rangle$ directions, respectively. The measured intensities of the diffracted neutrons are summed over multiple pixels that have the same coordinate along the horizontal detector axis. For details of the measured diffraction intensities, please see Supplemental information.

- Lines, M. E. & Glass, A. M. *Principles and Applications of Ferroelectrics and Related Materials*, Oxford University Press 2001.
- Burscu, E., Ravichandran, G. & Bhattacharya, K. Large strain electrostrictive actuation in barium titanate. *Appl. Phys. Lett.* **77**, 1698–1700 (2000).
- Damjanovic, D. Ferroelectric, dielectric and piezoelectric properties of ferroelectric thin films and ceramics. *Rep. Prog. Phys.* **61**, 1267–1324 (1998).
- Service, R. F. Shape-changing crystals get shifter. *Science* **275**, 1878 (1997).
- F. Li, F., Zhang, S., Xu, Z., Wei, X. & Shrout, T. R. Critical property in relaxor-PbTiO₃ single crystals- shear piezoelectric response. *Advanced Functional Materials* **21**, 2118 (2011).
- Schneider, G. A. & Heyer, V. Influence of the electric field on Vickers indentation crack growth in BaTiO₃. *J. Eur. Ceram. Soc.* **19**, 1299–1306 (1999).
- Nuffer, J., Lupascu, D. C. & Rödel, J. Damage evolution in ferroelectric PZT induced by bipolar electric cycling. *Acta Mater.* **48**, 3783–3794 (2000).
- Davis, M., Damjanovic, D., Hayem, D. & Setter, N. Domain engineering of the transverse piezoelectric coefficient in perovskite ferroelectrics. *J. Appl. Phys.* **98**, 014102 (2005).
- Bell, A. J. Phenomenologically derived electric field-temperature phase diagrams and piezoelectric coefficients for single crystal barium titanate under fields along different axes. *J. Appl. Phys.* **89**, 3907–3914 (2001).
- Wada, S., Suzuki, S., Noma, T., Suzuki, T., Osada, M., Kakihana, M., Park, S.-E., Cross, L. E. & Shrout, T. R. Enhanced piezoelectric property of barium titanate single crystals with engineered domain configurations. *Jpn. J. Appl. Phys.* **38**, 5505–5511 (1999).
- Fu, H. & Cohen, R. E. Polarization rotation mechanism for ultrahigh electromechanical response in single-crystal piezoelectrics. *Nature* **403**, 281–283 (2000).
- Davis, M., Budimir, M., Damjanovic, D. & Setter, N. Rotator and extender ferroelectrics: Importance to the shear coefficient to the piezoelectric properties of domain-engineered crystal and ceramics. *J. Appl. Phys.* **101**, 054112 (2007).
- Hook, R. E. & Hirth, J. P. The deformation behavior of isoaxial bicrystals of Fe-3% Si. *Acta Metall.* **15**, 535–551 (1967).
- Rys, J. Compatibility effects at the phase interfaces in duplex steel (α/γ) bicrystals. *J. Materials Processing Technology* **64**, 343–352 (1997).
- Martinez-Fernandez, J., Jimenez-Melendo, M. & Dominguez-Rodriguez, A. Ferroelasticity of the displacive tetragonal phase in Y₂O₃ partially stabilized ZrO₂ (Y-PSZ) single crystals. *J. Mater. Res.* **11**, 1972–1978 (1997).
- Dai, Z. R., Wang, Z. L., Duan, X. F. & Zhang, J. Linkup of 90 domain boundaries with interface dislocations in BaTiO₃/LaAlO₃. *Appl. Phys. Lett.* **68**, 3093–3095 (1996).
- McQuaid, R. G. P., McGilly, L. J., Sharma, P., Gruverman, A. & Gregg, J. M. Mesoscale flux-closure domain formation in single-crystal BaTiO₃. *Nature Comm.* DOI: 10.1038/ncomms1413.
- Nelson, C. T. *et al.* Domain dynamics during ferroelectric switching. *Science* **334**, 968–971 (2011).
- Catalan, G., Seidel, J., Ramesh, R. & Scott, J. F. Domain wall nanoelectronics. *Rev. Mod. Phys.* **84**, 119–156 (2012).
- Edwin Garcia, R., Huey, B. D. & Blendell, J. E. Virtual piezoforce microscopy of polycrystalline ferroelectric films. *J. Appl. Phys.* **100**, 064105 (2006).
- Holt, M., Hassani, K. h. & Sutton, M. Microstructure of ferroelectric domains in BaTiO₃ observed via X-ray microdiffraction. *Phys. Rev. Lett.* **95**, 085504 (2005).
- Rogan, R. C., Tamura, N., Swift, G. A. & Ustundag, E. Direct measurement of triaxial strain fields around ferroelectric domains using X-ray microdiffraction. *Nature Mat.* **2**, 379–381 (2003).
- Jo, Y. J. *et al.* Structural consequences of ferroelectric nanolithography. *Nano Lett.* **11**, 3080–3084 (2011).
- Yoneda, Y., Kohmura, Y., Suzuki, Y., Hamazaki, S.-i. & Takashige, M. X-Ray diffraction topography on a BaTiO₃ crystal. *J. Phys. Soc. Jpn.* **73**, 1050–1053 (2004).
- Durbin, M. K., Hicks, J. C., Park, S.-E. & Shrout, T. R. X-ray diffraction and phenomenological studies of the engineered monoclinic crystal domains in single crystal relaxor ferroelectrics. *J. Appl. Phys.* **87**, 8159–8164 (2000).
- Ohwada, K., Hirota, K., Rehrig, P. W., Fujii, Y. & Shirane, G. Neutron diffraction study of field-cooling effects on the relaxor ferroelectric Pb[(Zn_{1/3}Nb_{2/3})_{0.92}Ti_{0.08}]O₃. *Phys. Rev. B* **67**, 094111 (2003).
- Daniels, J. E. *et al.* Neutron diffraction study of the polarization reversal mechanism in [111]_c-oriented Pb(Zn_{1/3}Nb_{2/3})O₃-xPbTiO₃. *J. Appl. Phys.* **101**, 104108 (2007).
- Merz, W. Double hysteresis loop of BaTiO₃ at the curie point. *Phys. Rev.* **91**, 513–517 (1953).
- Wada, S. *et al.* Enhanced piezoelectric properties of barium titanate single crystals with different engineered-domain sizes. *J. Appl. Phys.* **98**, 014109 (2005).
- Hall, D. A., Steuwer, A., Chrdhirunkorn, B., Withers, P. J. & Mori, T. Texture of poled tetragonal PZT detected by synchrotron X-ray diffraction and micromechanics analysis. *Mat. Sci. Engin. A* **409**, 206–210 (2005).
- Hall, D. A., Steuwer, A., Cherdhirunkorn, B., Withers, P. J. & Mori, T. Micromechanics of residual stress and texture development due to poling in polycrystalline ferroelectric ceramics. *J. Mech. Phys. Solids* **53**, 249–260 (2005).
- Mura, T. *Micromechanics of Defects in Solids*, Martinus Nijhoff. *Dordrecht* (1987).
- Sebastian, M. T., Klapper, H. & Bolt, R. J. X-ray diffraction study of KTP (KTiOPO₄) crystals under a static electric field. *J. Appl. Cryst.* **25**, 274–280 (1992).
- Hytch, M. J., Putaux, J.-L. & Thibault, J. Stress and strain around grain-boundary dislocations measured by high-resolution electron microscopy. *Philos. Mag.* **86**, 4641–4656 (2007).
- Konstos, A. & Landis, C. M. Computational modeling of domain wall interactions with dislocations in ferroelectric crystals. *Int. J. Solids and Structures* **46**, 1491–1498 (2009).
- Wang, X. L., Holden, T. M., Rennich, G. Q., Stoica, A. D., Liaw, P. K., Choo, H. & Hubbard, C. R. VULCAN – The engineering diffractometer at the SNS. *Physica B* **385–386**, 673–675 (2006).

Acknowledgement

The neutron scattering measurements were carried out at the Spallation Neutron Source, which is operated with the support from the Division of Scientific User Facilities, Office of Basic Energy Sciences, US Department of Energy, under Contract No. DE-AC05-000022725 with UT-Battelle, LLC. Funding from a Laboratory Directed Research and Development Fund of Oak Ridge National Laboratory is acknowledged. JJ, DG, and GT acknowledge support for their contributions from the National Science Foundation through award number DMR-0746902 and the Department of the Army under contract number W911NF-09-1-0435. The authors also acknowledge technical assistance from Andre A. Parizzi and Daniel Maierhafer on High Voltage experimental setup.

Author contributions

AP, JJ, ADS and KA designed the experiments. AP, GT, DG and ADS conducted the experiments at the Oak Ridge National Laboratory. AP wrote the manuscript. All the authors were involved in scientific discussions and commented on the manuscript.

Additional information

Supplementary information accompanies this paper at <http://www.nature.com/scientificreports>

Competing financial interests: The authors declare no competing financial interests.

License: This work is licensed under a Creative Commons Attribution-NonCommercial-ShareAlike 3.0 Unported License. To view a copy of this license, visit <http://creativecommons.org/licenses/by-nc-sa/3.0/>

How to cite this article: Pramanick, A. *et al.* Strain incompatibility and residual strains in ferroelectric single crystals. *Sci. Rep.* **2**, 929; DOI:10.1038/srep00929 (2012).